Control design for a multi-regime 6-DOF underwater vehicle; development of MARIN's modular AUV

Bas J. de Kruif * **Hans Cozijn** * **Haite van der Schaaf** * **Egbert Ypma** *

* *Maritime Research Institute Netherlands (MARIN), The Netherlands (e-mail: b.j.d.kruif@marin.nl).*

Abstract: MARIN is designing and building a modular autonomous underwater vehicle (MAUV). The vehicle will serve as a platform for research projects to be carried out in our model test basins. The modular design will enable future extensions with additional sensors and actuators. The design of the vehicle and its control system is aimed at combining capabilities for position keeping (zero speed) and track sailing (medium and high speed). The vehicle is controlled in all 6 degrees of freedom, without any a-priori limitations.
This paper describes the control design of the MAUV. A feedback controller is designed and its robust stability analysed under parametric uncertainty and dynamic uncertainty due to the non-linear behaviour of its thrusters and the manoeuvring characteristics. As the system is not limited to small angles, the attitude is determined with quaternions to avoid singularities. Simulations show that the controlled system performs well at keeping its track, but currently the tracking performance degrades at at higher velocities.

Keywords: Autonomous underwater vehicles, robust stability, control design, quaternion feedback

1. INTRODUCTION

The Maritime Reasearch Intstitute Netherlands, MARIN, is designing and building an autonomous underwater vehicle (AUV). The vehicle will serve as a platform for research projects to be carried out in our model basins. The project foreseen with the AUV are concerned about i) the hydrodynamic forces acting on a relative small submersible vehicle over an extended speed range: ii) the influence of the control and actuators on this behaviour, and iii) research on autonomous systems in relation to other (autonomous) vessels.

As the intended use and its missions are diverse, the AUV has to be modular in design. The sensors, actuators and configurations of them should be interchangeable, while the software architecture should support this. The hardware and software design is detailed in (Cozijn et al., 2019). A CAD drawing of the system is shown in Fig. 1. The AUV is slightly longer than 3 meters, and is moved by 12 thrusters. The subject of this paper is the control design of the AUV. A 2-degree of freedom controller is proposed: a feedback controller to counter disturbances and give some minimal performance, even if there are unmodelled dynamics; and a (future) feed-forward controller to improve the (tracking) performance (Skogestad and Postlethwaite, 2007).

The feed-forward controller needs a model of the hydrodynamic and hydrostatic forces acting on the AUV. This information is yet unavailable and will be collected during the operation of the AUV. These values will be compared to the calculated values with CFD. A feedback controller is needed such that the AUV can move in a controlled way

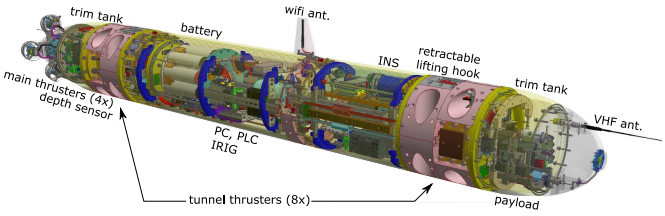

Fig. 1. A CAD drawing of the MAUV

in our model basins. A common approach for feedback control of an AUV is sliding mode control, see among others (Yoerger and Slotine, 1985; Breivik and Fossen, 2006). This approach incorporates the non-linear dynamics into the feedback controller. In order for the approach to work, the control model needs to be simplified such that all the states are measurable (Logan, 1994). A sliding mode controller can show chatter in the control signals if it is tuned incorrectly. As we plan to counter the non-linearities with a feed-forward controller in future work, incorporating them into a sliding mode controller is not needed, and a simpler controller without the possibility of this chatter is preferred.

Furthermore, as the missions can include both track sailing to an object of interest, and then the assessment of this object from different angles. The control should be able to accommodate fast sailing and 6 DOF low speed hovering. An example of this behaviour might occur at the detection and recognition of sea-mines. The AUV has to go to the mine, and then inspect the object from all possible angles. Hence, its attitude cannot be given in Euler angles as they

can become singular, known as the gimbal lock. In this work we use quaternions as described by Fossen (2011).

In this paper we will describe the design and analysis of a feedback controller that is robustly stable for unmodelled dynamics including the difference in behaviour at different velocities. Although this paper will focus on the design and analysis, the controller needs to be easy to tune when it is used for the actual AUV tests in our model basins.

In order to come to a controller, we start with the description of our control model in section 2. We want feedback from our global position and attitude, as well as from body fixed angular velocities. This means that we have to map the global forces and torques to body fixed forces and torques. A simple linear model results on which which we base our control design.

However, the system under investigation contains uncertainties and we need to analyse these to test if the controller remains stable. Some of these uncertainties stem from unknown parameters, such as added mass and damping. Another source of uncertainty is unmodelled dynamics. The Coriolis/centrifugal forces are dependent on the velocity but we model these as uncertainties. The same holds for the non-linear behaviour of the thrusters. A set of experiments to find an uncertainty model of the thruster is provided in section 3.

In section 4 a set of state feedback controllers is designed by means of pole placement. The robust stability of these controllers is tested on the uncertainty model of the AUV deduced in the previous section. A set of performance simulations is done on a detailed model to assess the performance of the selected controller.

2. CONTROL MODEL

In order to use linear techniques such as pole placement, a linear control model is required and a full state vector. The MAUV's state vector is available as the global positions are measured with a camera system in our towing tanks (Cozijn et al., 2019). A state feedback controller is used to utilise all this information. If the state is not measured, it can be estimated with a state estimator.

The equations of motion for a 6 DOF AUV are given as (Fossen, 2011):

$$\dot{\boldsymbol{\eta}} = \mathbf{J}_{\mathbf{q}}(\boldsymbol{\eta})\boldsymbol{\nu} \tag{1a}$$

$$\mathbf{M}\dot{\boldsymbol{\nu}} + \mathbf{C}(\boldsymbol{\nu})\boldsymbol{\nu} + \mathbf{D}(\boldsymbol{\nu})\boldsymbol{\nu} + \mathbf{g}(\boldsymbol{\eta}) = \boldsymbol{\tau}^{\mathrm{bf}}. \tag{1b}$$

In these equations, the vector $\boldsymbol{\eta}$ denotes the global position and attitude in quaternions, $\boldsymbol{\nu}$ the body fixed (angular) velocity, and $\boldsymbol{\tau}^{\mathrm{bf}}$ the body fixed actuator forces and torques. $\mathbf{M}, \mathbf{C}(\boldsymbol{\nu})$ and $\mathbf{D}(\boldsymbol{\nu})$ denote the mass, Coriolis/centripetal and the damping matrix, respectively. The added masses are included in these matrices. The vector $\mathbf{g}(\boldsymbol{\eta})$ represents the hydrostatic forces. The matrix $\mathbf{J}_{\mathbf{q}}(\boldsymbol{\eta})$ denotes the attitude dependent transformation matrix specified in quaternions. Eq. (1a) can be split into a part for translations and a part for rotations:

$$\dot{\boldsymbol{\eta}} = \begin{bmatrix} \dot{\boldsymbol{p}} \\ \dot{\boldsymbol{q}} \end{bmatrix} = \begin{bmatrix} \mathbf{R}_b^n(\boldsymbol{q})\boldsymbol{v} \\ \mathbf{T}_{\mathbf{q}}(\boldsymbol{q})\boldsymbol{\omega} \end{bmatrix} = \begin{bmatrix} \mathbf{R}_b^n(\boldsymbol{q})\boldsymbol{v} \\ \boldsymbol{q}\begin{bmatrix} 0 \\ \boldsymbol{\omega} \end{bmatrix} \end{bmatrix}, \tag{2}$$

in which the state $\boldsymbol{\eta}$ contains a position and a quaternion vector $\boldsymbol{p}$ and $\boldsymbol{q}$, and the state $\boldsymbol{\nu}$ is split in a velocity $\boldsymbol{v}$ and angular velocity $\boldsymbol{\omega}$ part. $\mathbf{R}_b^n(\boldsymbol{q})$ denotes the rotation matrix formed from quaternions, and $\mathbf{T}_{\mathbf{q}}(\boldsymbol{q})$ the transformation from angular velocities to quaternion derivatives. Both matrices are given in (Fossen, 2011). The last equality can be found by comparing the matrix $\mathbf{T}_{\mathbf{q}}(\boldsymbol{q})$ with the quaternion multiplications, see among others (Dam et al., 1998; Jensen and Wisniewski, 2001; Graf, 2008).

We define the error for the translational part as:

$$\boldsymbol{e}_{\mathrm{t}} = (\mathbf{R}_b^n)^T \left(\boldsymbol{p}_{\mathrm{sp}} - \boldsymbol{p}\right), \tag{3}$$

then the error dynamics for a constant reference position becomes:

$$\dot{\boldsymbol{e}}_{\mathrm{t}} = \left(\dot{\mathbf{R}}_b^n\right)^T \left(\boldsymbol{p}_{\mathrm{sp}} - \boldsymbol{p}\right) - (\mathbf{R}_b^n)^T \dot{\boldsymbol{p}} \tag{4a}$$

$$= S(\boldsymbol{\omega})^T (\mathbf{R}_b^n)^T \left(\boldsymbol{p}_{\mathrm{sp}} - \boldsymbol{p}\right) - (\mathbf{R}_b^n)^T \mathbf{R}_b^n \boldsymbol{v} \tag{4b}$$

$$= -\left(\boldsymbol{\omega} \times \boldsymbol{e}_{\mathrm{t}}\right) - \boldsymbol{v}, \tag{4c}$$

in which $S(\boldsymbol{\omega})$ is the cross product matrix. Equivalently, if we define the error for the rotational part as:

$$\boldsymbol{e}_{\mathrm{r}} = 2\mathbf{P}\log(\bar{\boldsymbol{q}}\boldsymbol{q}_{\mathrm{sp}}). \tag{5}$$

In this equation $\mathbf{P}$ is a 3×4 matrix that selects the last three elements of the quaternion. For a *unit* quaternion, the logarithm of a quaternion results in $\log(\boldsymbol{q}) = [0, \alpha\boldsymbol{n}]$ (Dam et al., 1998). Rotation of an angle α over the Euler axis $\boldsymbol{n}$ is similar as the rotation provided by the quaternion $\boldsymbol{q}$. Hence, this error indicates the angle and axis over which the MAUV has to rotate to come to the set point attitude. With this error, the error dynamics become:

$$\dot{\boldsymbol{e}}_{\mathrm{r}} = 2\mathbf{P}\frac{1}{\bar{\boldsymbol{q}}\boldsymbol{q}_{\mathrm{sp}}}\dot{\bar{\boldsymbol{q}}}\boldsymbol{q}_{\mathrm{sp}} = 2\mathbf{P}\overline{\left(\bar{\boldsymbol{q}}\boldsymbol{q}_{\mathrm{sp}}\right)}\dot{\bar{\boldsymbol{q}}}\boldsymbol{q}_{\mathrm{sp}} \tag{6a}$$

$$= 2\mathbf{P}\bar{\boldsymbol{q}}_{\mathrm{sp}}\boldsymbol{q}\dot{\bar{\boldsymbol{q}}}\boldsymbol{q}_{\mathrm{sp}} = -\mathbf{P}\bar{\boldsymbol{q}}_{\mathrm{sp}}\begin{bmatrix} 0 \\ \boldsymbol{\omega}^{\mathrm{ef}} \end{bmatrix}\boldsymbol{q}_{\mathrm{sp}} \tag{6b}$$

$$= -\mathbf{P}\begin{bmatrix} 0 \\ \boldsymbol{\omega} \end{bmatrix} = -\boldsymbol{\omega}. \tag{6c}$$

$\boldsymbol{\omega}^{\mathrm{ef}}$ is the earth fixed angular velocity. The body fixed rotation in the set point frame is equal to the rotation in the ship fixed frame *for this rotation*, as the rotation is around the Euler axis from the ship fixed frame to the set point frame. This allows for the transition from (6b) to (6c). The combined error dynamics become:

$$\dot{\boldsymbol{e}} = \begin{bmatrix} \dot{\boldsymbol{e}}_{\mathrm{t}} \\ \dot{\boldsymbol{e}}_{\mathrm{r}} \end{bmatrix} = \begin{bmatrix} \left(\boldsymbol{\omega} \times \boldsymbol{e}_{\mathrm{t}}\right) - \boldsymbol{v} \\ -\boldsymbol{\omega} \end{bmatrix} \tag{7a}$$

$$\mathbf{M}\dot{\boldsymbol{\nu}} + \mathbf{C}(\boldsymbol{\nu})\boldsymbol{\nu} + \mathbf{D}(\boldsymbol{\nu})\boldsymbol{\nu} + \mathbf{g}(\boldsymbol{\eta}) = \boldsymbol{\tau}^{\mathrm{bf}} \tag{7b}$$

As we will move with relative slow speed and want our damping from the controller, not from the physical damping, the Coriolis/centripetal forces will be neglected, and we will design our controller with the damping matrix set to zero. The first term on the right hand side of (7a) can be compensated for by applying an additional force, and will be therefore ignored for the rest of the work. Finally, the MAUV is designed to have the buoyancy point at the centre of gravity, possible with the help of the ballast tanks. This will result in small gravitational forces. The errors that are introduced by these assumptions are countered by

Table 1. UV properties and velocity range.

mass [kg] or [kgm^2]	added mass [kg] or [kgm^2]	damping N/(m·s)] or [N/(rad·s)]	velocity [m/s] or [rad/s]
$m = 236$	$X_{\dot{u}} = 40.0 \pm 10\%$	$X_u = 5 \pm 25\%$	$u = [-0.25, 1.0]$
$m = 236$	$Y_{\dot{v}} = 200 \pm 10\%$	$Y_v = 7.5 \pm 25\%$	$v = [-0.2, 0.2]$
$m = 236$	$Z_{\dot{w}} = 200 \pm 10\%$	$Z_w = 7.5 \pm 25\%$	$w = [-0.2, 0.2]$
$I_{xx} = 6.6$	$K_{\dot{p}} = 0.0 - 5.0$	$K_p = 5 \pm 25\%$	$p = [-0.2, 0.2]$
$I_{yy} = 213$	$M_{\dot{q}} = 125.0 \pm 10\%$	$M_q = 7.5 \pm 25\%$	$q = [-0.2, 0.2]$
$I_{zz} = 213$	$N_{\dot{r}} = 125.0 \pm 10\%$	$N_r = 7.5 \pm 25\%$	$r = [-0.2, 0.2]$

introducing uncertainty in the model, as will be discussed in the next section. The feedback law can be designed with linear control as $\boldsymbol{\tau}^{\text{bf}} = \mathbf{K}\boldsymbol{e}$. The advantage of using the transformed output, is that especially for the rotations, we lost the non-linear term with the unity constraint on its magnitude.

3. UNCERTAINTY MODELLING

The state controller does not explicitly incorporate the uncertainty in its design. We want our feedback system stable for uncertain effects, and in the next section the robust stability against the uncertainties is analysed. Two sources of uncertainty are considered: i) parametric uncertainty and ii) dynamic uncertainty.

3.1 parametric uncertainty

The parametric uncertainties can directly be used in the equation of motion. The values of the parameters as well as their assumed uncertainties are given in Table 1. The uncertainty of the mass and added mass is combined in the uncertainty for the added mass. The uncertainty in the damping is chosen to encompass both the linear and the quadratic damping terms. They are modelled as uncertainty, and are not treated as velocity dependent.

The controller does not incorporate the actual velocity, but it should be stable for the velocity ranges during operation. The Coriolis matrix $\mathbf{C}(\boldsymbol{\nu})$ is velocity dependent, and changes the behaviour of the system due to its velocity. The AUVs velocity is therefore modelled as an uncertain parameter that influences the matrix $\mathbf{C}(\boldsymbol{\nu})$.

Several velocity ranges are used to test at what speed the robust stability becomes a problem. Next to the first range given in the table, the second range sets the maximum surge velocity at 0.25 m/s, the third range bounds all the velocities between -0.1 – 0.1 m/s, and the last range makes all the velocities equal to zero.

3.2 dynamic uncertainty

Next to a set of parametric uncertainty, we have a dynamic uncertainty due to the use of thrusters. A set of Blue Robotics T200 thrusters is used to deliver thrust to the AUV. These thrusters were equipped with hall sensors to tightly control their angular velocity. The thruster dynamics are dependent on the rotational velocity of the thrusters as well as on the water speed relative to the propeller blades, as noted in (Yoerger and Slotine, 1985; Healey et al., 1995). We want to identify the generated thrust as function of frequency at different rotational

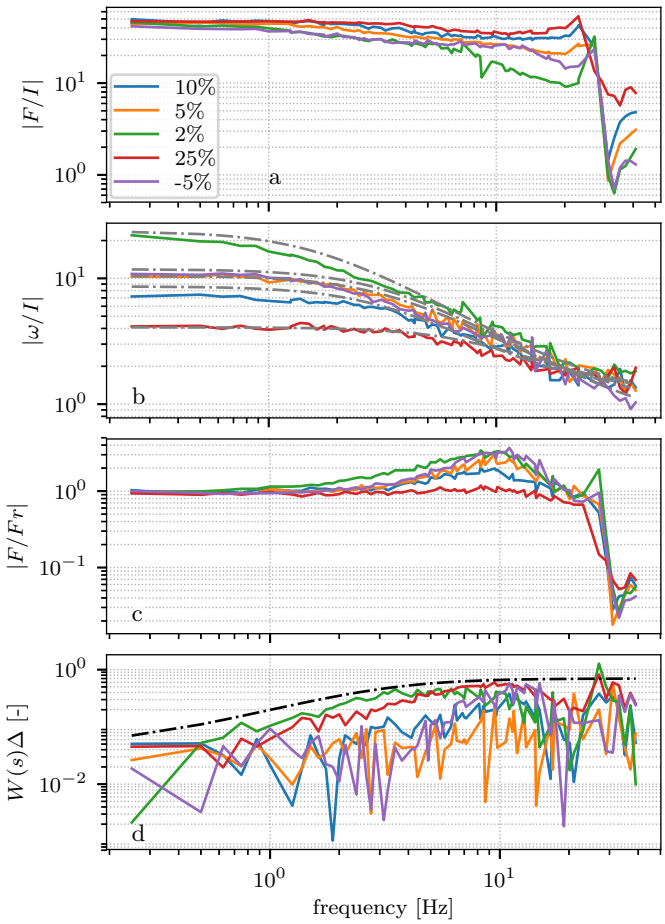

Fig. 2. The response of the thrust and the rotational velocity due to driving motor torque. Different offset torques are shown.

velocities. Again, the state feedback controller does not incorporate this information, so we model it as uncertainty.

A single thruster, disassembled from the MAUV, is connected to a fixed thrust sensor and placed in our basin. The basin's length of 250 m minimises the chance of residual flow. The thruster is not moving. A constant electrical current, related to a constant motor torque, is applied to the thruster. A set of sinusoid currents are superimposed on this. The amplitude of these sinusoids was chosen as small as possible, but still resulting in a clear response. The direction of rotation did not change during the experiment. The excitation is known as multisines (Pintelon and Schoukens, 2012).

The thrust, F, current, I, and angular velocity, ω, were measured at 100 Hz. The amplification at the excitation frequencies for current to thrust and current to RPM were calculated. The results of these amplifications are shown in Fig. 2a and b. The response for several current offsets are shown in this figure.

Fig. 2a shows that the thrust at low frequencies is nearly independent from the motor torque, i. e. the motor torque is proportional to the motor current. This behaviour corresponds with the above cited literature. The dry friction will give some small differences though. The thrust is also known to be quadratically related to the angular

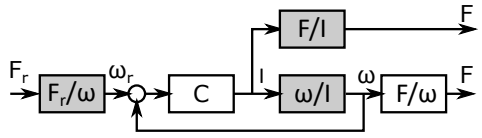

Fig. 3. scheme to calculate the thrust based on the requested thrust. Gray blocks are known. The lead-lag controller is designed to have a bandwidth of 10 Hz

velocity. The angular velocity *amplification* will therefore be smaller for larger motor torques. This can be observed in Fig. 2b.

The dynamic response is measured for a positive and negative direction at 5% of the motor current. These lines fall on top of each other. There is no directional difference in the dynamic response. There was a small difference observed in the steady state response, although these measurements are not shown here.

Furthermore, a resonance – anti-resonance can be seen in the transfer from the motor torque to the force at 20 and 30 Hz. This is attributed to the stiffness in the measurement system (Koster et al., 1998). A vibration around that frequency was also observed when the mechanical system was hit before the experiments.

The angular velocity of the thrusters will be controlled during the operation of the AUV to compensate for the dry friction. The relation between steady state angular velocity and thrust is known to be quadratic, and its coefficient has been measured. The uncertainty between the thrust and requested thrust needs to be determined. Refer to Fig. 3. The grey blocks in this figure were measured.

Based on the transfer from current to thrust, $|F/I|$, and current to RPM, $|\omega/I|$, we can construct the relation between thrust and RPM, $|F/\omega|$, the utmost right white block. This can be done by dividing the magnitude of the transfer function of Fig. 2a by 2b for each frequency f_i as:

$$\left|\frac{F(f_i)}{\omega(f_i)}\right| = \left|\frac{F(f_i)}{I(f_i)}\right| \Big/ \left|\frac{\omega(f_i)}{I(f_i)}\right|. \tag{8}$$

As we will control the angular velocity of the thrusters during the operation of the AUV, the next step is to determine the response of the RPM to the requested RPM. For this, we fit the response ω/I with a first order response so that we also have the phase of the transfer function. These fits are shown in Fig. 2b as dashed lines. A simple lead-lag controller tuned at 10 Hz is used to control the thruster. The controller is based on the fitted coefficients is:

$$C(s) = \frac{20s + 20}{s^2 + 10.1s + 0.1}. \tag{9}$$

Finally, at zero frequency, we know how the thrust is quadratically related to the RPM for each of these offsets, $|F_r(0)/\omega(0)|$. With this relation, the requested torque and the delivered torque can be made identical at steady state conditions. With the closed loop response and the calculated transfer from RPM to thrust, we can calculate the graphs in Fig. 2c for the requested thrust to actual thrust.

For the uncertainty analysis the transfer between thrust and requested thrust is modelled as a first order response with multiplicative uncertainty. This fitted Fig. 2b well for a first order transfer function:

$$\left|\frac{F}{F_\mathrm{r}}\right| = \frac{15\pi}{s + 15\pi}(1 + W(s)\Delta(s)) \tag{10}$$

The realisations from the measurements for $W(s)\Delta$ are shown in Fig. 2d. In this figure we can see that the uncertainty at low frequencies is approximately 5%. The uncertainty at the bandwidth of the controlled system peaks at 75%. After the bandwidth, the uncertainty depends on the surrounding, but for this open water test it remains at 75%. The uncertainty is modelled as:

$$W(s) = \frac{\tau s + r_0}{(\tau/r_\infty)s + 1},\ \|\Delta(s)\|_\infty \leq 1, \tag{11}$$

with $\tau = 1/5, r_0 = 0.05,\ r_\infty = 0.75$. The weighing matrix is plotted in Fig. 2d as a black dashed line. The body fixed forces in the equation of motion are pre-multiplied with this uncertainty model.

4. CONTROL DESIGN

The sensors in the AUV measure the global position, attitude and body fixed (angular) velocities. We use these signals to design a state feedback controller. The gains are calculated for low speeds, and we want the damping from the controller, so we set the damping matrix in the design model to zero. The thruster dynamics are not used in the design, which will limit the upper bandwidth. The poles are placed with Matlab's pole placement algorithm. A set of controllers is designed with increasing location of the poles, and hence bandwidth. The poles are located at the same (negative) real location for each individual controller in the set. Although the poles associated with the body fixed velocities deviate 1% as the pole placement algorithm could not handle the multiplicity of the pole location.

For each of these controllers the robust stability is tested as described in (Skogestad and Postlethwaite, 2007) with Matlab's `mussv` command. The uncertainty is structured, and is treated as such. The model for the equations of motion are pre-multiplied with the uncertainty model of the thrusters. The model equations (7) are used for this.

The maximum value of upper bound of the μ-norm for the set of controllers is shown in Fig. 4. The value of the norm should be below one for *guaranteed* robust stability. If it is larger than one, it is not guaranteed to be stable. The norm is calculated for four velocities as told in section 3.1. The upper bound of the μ-norm as function of frequency at $u_x = 0.25$ is shown in Fig. 5 for some of the controllers. The bold line corresponds to a pole placement at -1, and is below one for all the frequencies.

Interesting to note is that there is a minimal needed bandwidth of the controller before the system becomes robustly stable, even if the system is nominally stable. Inspection of Fig. 5 shows two peaks, especially clear for a pole placement at -0.1. These occur at high (forward) velocity. If all the velocities are set to 0.25 [m/s] and 0.25 [rad/s], and the controller poles are placed at -1, then the corresponding output motion can be found from the singular value decomposition of the response at that frequency. The first mode corresponds to a motion in y, and z direction, with an accompanying rotation

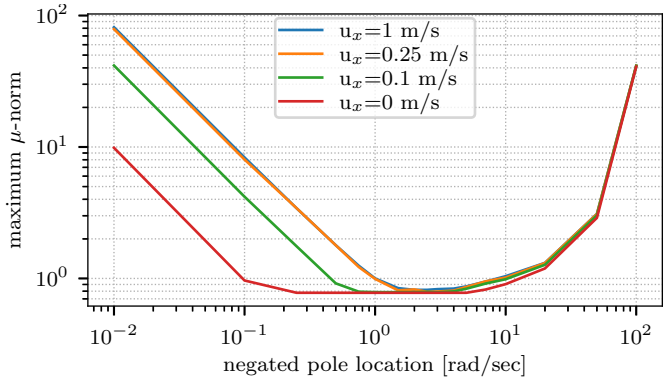

Fig. 4. maximum μ-norm as function of the pole location. Four settings for forward velocity are used

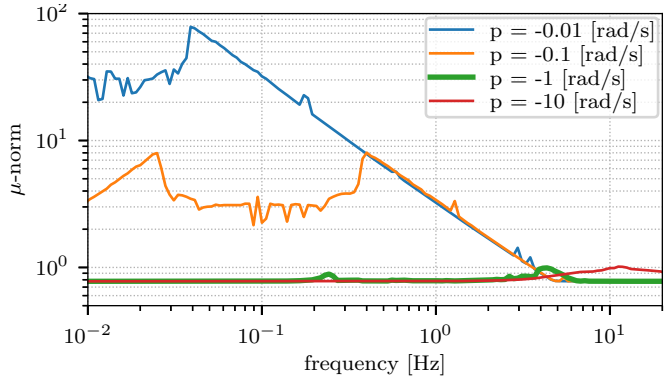

Fig. 5. μ-norm as function of frequency for several pole placement locations.

around these axes. The AUV is wagging its tail. The second mode corresponds to a rotation around the x axis. The saturation due to the thrusters' maximum velocity can further degenerate the performance. The rotation and translation in the y, and z direction can also be explained due to the large negative Munk moment for this hydrodynamic design. The (added) mass in x direction is much smaller than the (added) mass in y, and z-direction.

If the velocity is decreased, these vibrational modes become less prominent. A lower bandwidth becomes enough to counter the effect, as can be seen in Fig. 4. On the other hand, if the bandwidth becomes too large, then the uncertainty in the thruster dynamics limits the robust stability. Fig. 5 shows that for higher bandwidths the μ-norms maximum value occurs at the frequencies at which the thrusters uncertainty is large.

These results lead to a tuning approach for when the AUV is tested in the basins: start at low velocities and increase the bandwidth of the controller until the thruster cannot cope with the control signals. Then we can increase the velocity until the AUV cannot keep its course. This is the maximum velocity. This tuning can be done when the system is tested in the basins.

5. PERFORMANCE SIMULATION

The controller is tested on a *simulation* model of the AUV. The simulation model is a detailed version of the control model. The simulation runs in XMF, an in-house simulation suite for marine vessels and structures with an emphasis

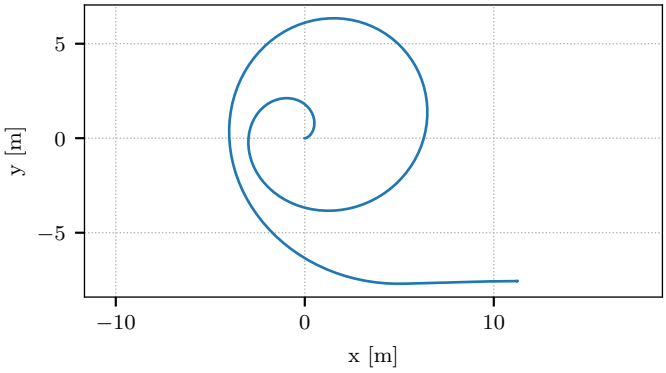

Fig. 6. Top view of the path to test the control performance. After the spiral, the AUV decreases its forward velocity while it simultaneously goes up for 1 m.

on hydrodynamic validated models (Ypma and Abbing, 2012). The effects that are incorporated in the simulations are the hydrostatics based on the 3D CAD design of the AUV. Furthermore, the interaction between the flow direction and the thrusters is included (Karlikov and Sholomovich, 1998), as well as the measured thrust and torque for specified angular velocity in an identification experiment. For more details, see (Cozijn et al., 2019). The calculated damping and added mass are estimated based on an empirical manoeuvring model, and are included in the simulation model as well.

The path as shown in Fig. 6 is used as desired track for the AUV to follow. At each time step, the global positons and body fixed velocities are provided. Along this path, the forward velocity increases linearly, and a lateral velocity is added as if it has to compensate for a global current field. The turning rate is kept constant. After two circles, the AUV brakes, and moves one meter in the direction of the surface. This cannot be seen in Fig. 6, but it is shown in the set points as function of time in Fig. 7. The maximal surge velocity is set to 0.5 m/s, the maximum sway velocity to 0.1 m/s and the yaw rate to $2\pi/100$ rad/sec. This track is selected to show the increase in error due to the forward velocity. The controller is tuned by increasing the bandwidth as described in previous section. The poles were placed at -1. For larger values the thrusters had difficulties generating the required thrust in a timely fashion, and the simulation time step started to become prohibitively small to simulate the stiff system.

Fig. 7 and 8 show the translational behaviour of the AUV and the accompanying error. The dashed lines show the reference signal, and the solid lines the measured signals. The tracking of the path is as expected: at lower velocities the path is tracked correctly, while at higher forward speeds the tracking error increases. The attitude behaviour is not shown here, but behaves similarly. The position as well as the attitude based on the quaternions are tracked and remain stable in this velocity range. A jump in the error can be observed at $t \approx 200$ s, which is caused in a jump in the acceleration.

6. CONCLUSION

In this paper a feedback controller is designed for the control of an AUV. It is based on a pole placement al-

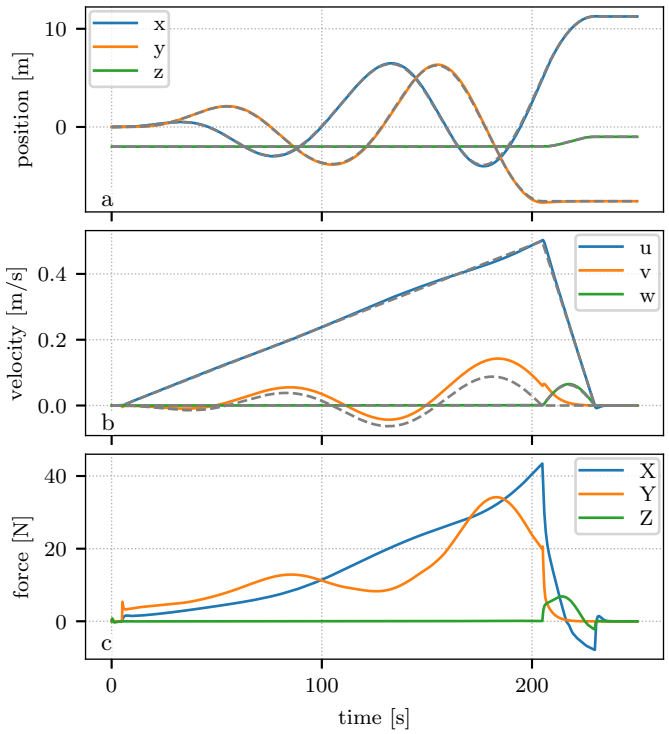

Fig. 7. Translational behaviour of the AUV. The dashed lines show the setpoints, and the solid lines denote the measurements.

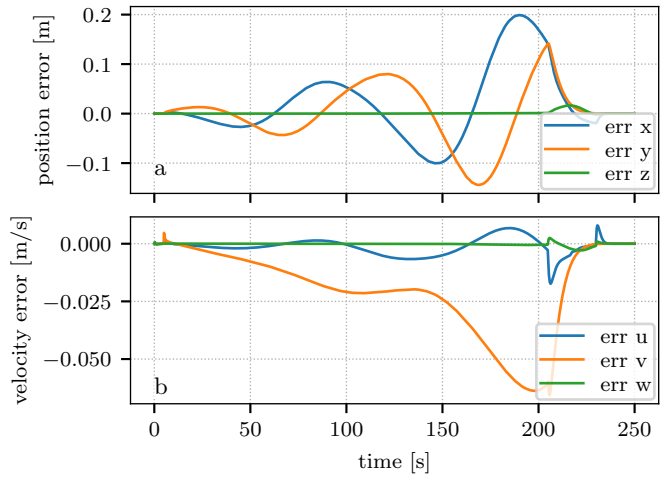

Fig. 8. Errors in position and velocity accompanying Fig. 7

gorithm and uses the global position and attitude signals to get the system to where it needs to be. It uses the body fixed (angular) velocity signals to realise damping. All the attitude are specified in quaternions, so that all attitudes are possible without the possibility of a gimbal lock. The control has been tested on a detailed simulation model, and the system was capable of tracking its path.

The controller will be used when the AUV is tested in our basins. One of these tests will be to determine the hydrodynamic coefficients for a feed forward controller. For this aim, it is important that the system is robustly stable for the uncertainties in the model, as well as general unmodelled dynamics. This has been tested, and for limited velocities the system is robustly stable. For larger velocities it was not guaranteed to be stable, nor guaranteed to be unstable. The bandwidth of the controller is bound from below by the vibrational modes due to the Coriolis/centrifugal forces: the AUV starts to wag. The bandwidth of the controller is limited from above due to the uncertainty in the thrusters. This allows for simple tuning of the controller: increase the bandwidth at low velocities until the thrusters cannot cope with the commands any more. The controller is implemented in our in-house simulation environment. Due to the split of the controller and the ship model, we can directly use the developed controller on the real AUV. This allows us to start researching the hydrodynamic effect acting on an AUV the moment the hardware is finished.

REFERENCES

Breivik, M. and Fossen, T.I. (2006). A unified control concept for autonomous underwater vehicles. In *American Control Conference, 2006*, 7—-pp. IEEE.

Cozijn, J.L., van der Schaaf, H., de Kruif, B.J., and Ypma, E. (2019). Design of an underwater vehicle for use in basin experiments, development of marin's modular auv. In *CAMS'19*, (accepted).

Dam, E.B., Koch, M., and Lillholm, M. (1998). Quaternions , Interpolation and Animation. Technical report, University of Copenhagen, Copenhagen.

Fossen, T.I. (2011). *Handbook of marine craft hydrodynamics and motion control*. John Wiley & Sons.

Graf, B. (2008). Quaternions and dynamics. -. URL `http://arxiv.org/abs/0811.2889`.

Healey, A.J., Rock, S.M., Cody, S., Miles, D., and Brown, J.P. (1995). Toward an improved understanding of thruster dynamics for underwater vehicles. *IEEE Journal of oceanic Engineering*, 20(4), 354–361.

Jensen, H.C. and Wisniewski, R. (2001). Quaternion feedback control for rigid-body spacecraft. In *AIAA Guidance, Navigation, and Control Conference and Exhibit*, 4338.

Karlikov, V.P. and Sholomovich, G.I. (1998). Some features of body-flow interaction in the presence of transverse jets. *Fluid dynamics*, 33(3), 313–317.

Koster, M.P., van Luenen, W.T.C., and de Vries, T.J.A. (1998). Mechatronica. -.

Logan, C.L. (1994). A comparison between H∞/μ-synthesis control and sliding-mode control for robust control of a small autonomous underwater vehicle. In *AUV'94.*, 399–416. IEEE.

Pintelon, R. and Schoukens, J. (2012). *System Identification: A Frequency Domain Approach, Second Edition*. IEEE Press, 2nd edition. doi:10.1002/9781118287422.

Skogestad, S. and Postlethwaite, I. (2007). *Multivariable feedback control: analysis and design*, volume 2. Wiley New York.

Yoerger, D. and Slotine, J. (1985). Robust trajectory control of underwater vehicles. *IEEE Journal of Oceanic Engineering*, 10(4), 462–470.

Ypma, E. and Abbing, A. (2012). 'XMF' - A software cooperation platform, a MARIN proposal for the CRS. Technical report, MARIN.